Phase Behavior and 13 C NMR Spectroscopic Analysis of the Mixed Methane + Ethane + Propane Hydrates in Mesoporous Silica Gels

ARTICLE *in* THE JOURNAL OF PHYSICAL CHEMISTRY B · OCTOBER 2010

Impact Factor: 3.3 · DOI: 10.1021/jp108037m · Source: PubMed

Phase Behavior and ^{13}C NMR Spectroscopic Analysis of the Mixed Methane + Ethane + Propane Hydrates in Mesoporous Silica Gels

Seungmin Lee, Inuk Cha, and Yongwon Seo*

Department of Chemical Engineering, Changwon National University, 9 Sarim-dong, Uichang-gu, Changwon-si, Gyeongnam 641-773, Republic of Korea

Received: August 25, 2010; Revised Manuscript Received: October 4, 2010

In this study, the phase behavior and quantitative determination of hydrate composition and cage occupancy for the mixed $CH_4 + C_2H_6 + C_3H_8$ hydrates were closely investigated through the experimental measurement of three-phase hydrate (H)−water-rich liquid (L_W)−vapor (V) equilibria and ^{13}C NMR spectra. To examine the effect of pore size and salinity, we measured hydrate phase equilibria for the quaternary CH_4 (90%) + C_2H_6 (7%) + C_3H_8 (3%) + water mixtures in silica gel pores of nominal diameters of 6.0, 15.0, and 30.0 nm and for the quinary CH_4 (90%) + C_2H_6 (7%) + C_3H_8 (3%) + NaCl + water mixtures of two different NaCl concentrations (3 and 10 wt %) in silica gel pores of a nominal 30.0 nm diameter. The value of hydrate−water interfacial tension for the CH_4 (90%) + C_2H_6 (7%) + C_3H_8 (3%) hydrate was found to be 47 ± 4 mJ/m^2 from the relation of the dissociation temperature depression with the pore size of silica gels at a given pressure. At a specified temperature, three-phase H−L_W−V equilibrium curves of pore hydrates were shifted to higher pressure regions depending on pore sizes and NaCl concentrations. From the cage-dependent ^{13}C NMR chemical shifts of enclathrated guest molecules, the mixed CH_4 (90%) + C_2H_6 (7%) + C_3H_8 (3%) gas hydrate was confirmed to be structure II. The cage occupancies of each guest molecule and the hydration number of the mixed gas hydrates were also estimated from the ^{13}C NMR spectra.

Introduction

Gas hydrates are nonstoichiometric crystalline compounds formed when "guest" molecules of suitable size and shape are incorporated in the well-defined cages in the "host" lattice made up of hydrogen-bonded water molecules. These compounds exist in three distinct structures, structure I (sI), structure II (sII), and structure H (sH), which contain differently sized and shaped cages.[1] Gas hydrates are of particular concern in the petroleum industry as well as in energy and environmental fields. Vast quantities of natural gas hydrates exist in permafrost regions or beneath deep oceans.[1] These naturally occurring gas hydrates are composed of a mixture of hydrocarbons, such as CH_4, C_2H_6, and C_3H_8, and nonhydrocarbons, such as hydrogen sulfide, carbon dioxide, and nitrogen, although their compositions are dependent on the origin (biogenic or thermogenic) and location of natural gas hydrate reservoirs. Each of these components has its own structural characteristics and hydrate phase equilibrium conditions. CH_4, a major component of natural gas hydrate, and C_2H_6 are known to form sI hydrate and need a relatively higher pressure for gas hydrate formation, whereas C_3H_8 forms sII hydrate at a much lower pressure.[1] Complex phase behavior and structural characteristics as well as the quantitative determination of cage occupancies for natural gas hydrates should first be considered in understanding and predicting hydrate stability zones in deep ocean sediment.

Natural gas hydrates beneath deep oceans, which are regarded as future energy resources, are commonly found in sand or clay-type sediments.[1] Natural gas hydrates in large pores of coarse-grained sand sediment have almost the same equilibrium pressure for hydrate dissociation and thermodynamic properties as that in the pure bulk water phase. However, the pore effect due to the geometrical constraints is not negligible when considering the natural gas hydrate in the sediments of fine-grained sand or clay-type sediments. In addition, the stability conditions of the natural gas hydrate in the deep ocean sediment are also affected by electrolytes dissolved in the seawater. A detailed and systematic investigation of the phase equilibria of natural gas hydrates is very important in exploring and exploiting natural gas hydrates in the deep ocean sediment because the phase equilibrium is closely related with the formation/dissociation conditions and stability region of natural gas hydrates. Therefore, it becomes essential to consider the complicated effects of both pore size and salinity on the stability conditions of natural gas hydrates. Phase equilibrium studies covering separately either pore size or salinity effect have been extensively conducted by many researchers,[2−9] and recently, some limited works concerning the combined effects of both pores and electrolytes on the formation of simple gas hydrates and mixed gas hydrates with two guests have been reported.[10−12] However, to the best of our investigation, despite the importance and urgency of the experimental data, no research on the phase equilibrium and structure analysis of natural gas hydrates containing both multiguest components and electrolytes in narrow pores appears in the literature.

Therefore, we attempted to investigate highly complex phase behavior and structural characteristics of pore gas hydrates containing both multiguest components and electrolytes. In the present study, a gas mixture of CH_4 (90%) + C_2H_6 (7%) + C_3H_8 (3%), which is a typical composition of natural gas hydrates, is chosen for multiguest components and NaCl for electrolytes. First, the hydrate phase equilibria for the quaternary CH_4 (90%) + C_2H_6 (7%) + C_3H_8 (3%) + water mixtures in silica gel pores of nominal diameters of 6.0, 15.0, and 30.0 nm were measured to examine the pore-size effect on the stability of natural gas hydrates. Second, the hydrate phase equilibria

* To whom correspondence should be addressed. Tel.: +82-55-213-3757. Fax: +82-55-283-6465. E-mail: yseo@changwon.ac.kr.

10.1021/jp108037m
Published on Web 10/21/2010

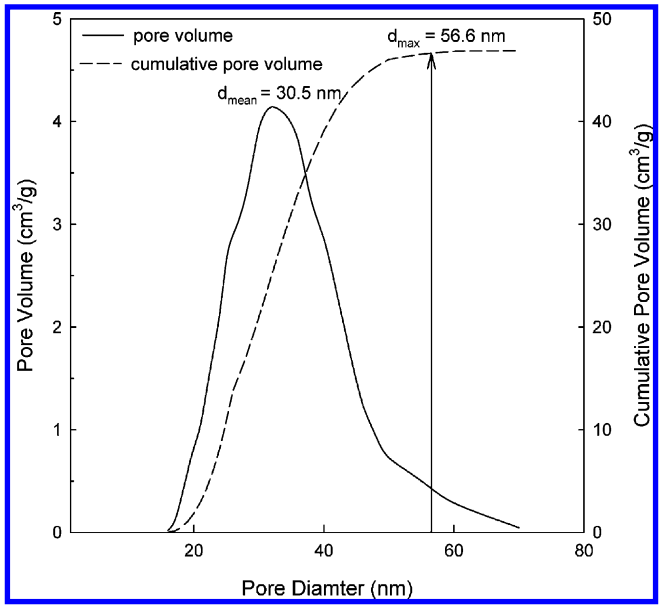

Figure 1. Pore-size distribution and cumulative pore-size distribution of nominal 30.0 nm silica gel.

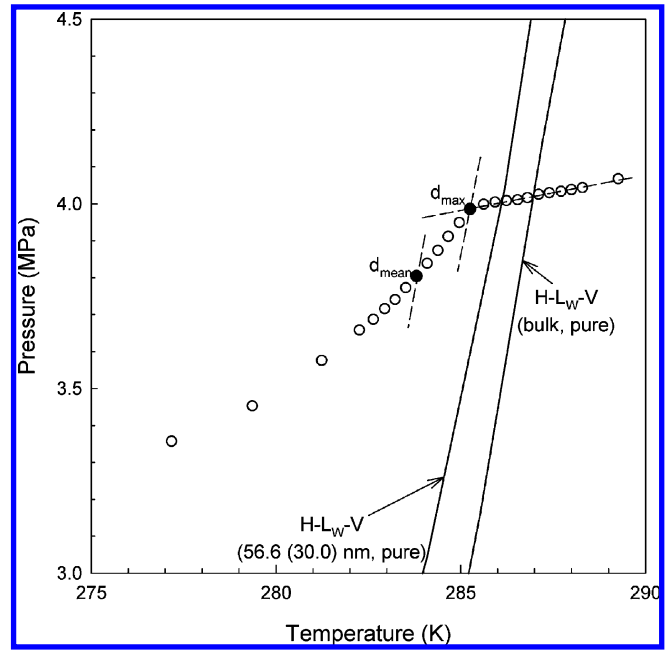

Figure 2. P versus T heating curve for the CH_4 (90%) + C_2H_6 (7%) + C_3H_8 (3%) + NaCl (3 wt %) + water mixtures in 56.6 (30.0) nm silica gel pores.

for the quinary CH_4 (90%) + C_2H_6 (7%) + C_3H_8 (3%) + NaCl + water mixtures were measured in nominal 30.0 nm silica gel pores at two different NaCl concentrations of 3 and 10 wt % to investigate the combined effect of pores and electrolytes. Finally, the ^{13}C NMR spectra were obtained to identify the hydrate structure and to estimate the cage occupancies of guests in the mixed CH_4 (90%) + C_2H_6 (7%) + C_3H_8 (3%) gas hydrates.

Experimental Section

Materials. The mixed CH_4 (90%) + C_2H_6 (7%) + C_3H_8 (3%) gas used for the present study was supplied by Gyeongdong Industrial Gas Co. (Korea). Silica gels of nominal pore diameters of 6.0 and 15.0 nm were purchased from Aldrich Co. (USA). Silica gel of a nominal pore diameter of 30.0 nm was purchased from Silicycle Co. (Canada). All materials were used without further treatment. The properties of silica gels having three different pore diameters were measured by ASAP 2420 and Autopore IV 9520 (Micromeritics, USA). Figure 1 shows the pore-size distribution and cumulative pore-size distribution of a nominal 30.0 nm silica gel sample. As shown in Figure 1, the maximum pore diameter of each silica gel sample was determined as the pore diameter corresponding to a 99.5% value of each final cumulative pore volume. The maximum pore diameters of nominal 6.0, 15.0, and 30.0 nm silica gels were found to be 12.9, 22.6, and 56.6 nm, respectively. Hereafter, for clarity, the silica gel sample will be expressed as the maximum diameter (nominal diameter) in the text, for example 56.6 (30.0) nm. More details of silica gel properties were given in the previous papers.[6,12]

Apparatus and Procedure. To prepare the pore-saturated silica gels, such that water or electrolyte solutions exist only within pores, the silica gels were first dried at 393 K for 24 h before water sorption. Some amount of dried silica gel powder was placed in a bottle, and an amount of water or electrolyte solutions identical to the pore volume of silica gel was added to the powder. After mixing, the bottle was sealed off with a cap to prevent water evaporation. Then, the bottle was vibrated with an ultrasonic wave at 293.15 K for 24 h to completely fill the pores with water or electrolyte solutions.

The experimental apparatus for hydrate phase equilibria was specially designed to accurately measure the hydrate dissociation pressures and temperatures. The equilibrium cell was made of 316 stainless steel and had an internal volume of about 150 cm^3. The experiment for hydrate-phase equilibrium measurements began by charging the equilibrium cell with about 80 cm^3 of silica gels containing pore water or electrolyte solutions. After the equilibrium cell was pressurized to the desired pressure with mixed CH_4 (90%) + C_2H_6 (7%) + C_3H_8 (3%) gas, the whole main system was slowly cooled to a temperature lower than the expected equilibrium temperature. When pressure depression due to hydrate formation reached a steady-state condition, the cell temperature was increased in 0.3 K steps of 2 h equilibrium time for samples of all pore sizes used in this study, which was confirmed to be sufficient by checking pressure (P) versus time (t) curves for each step.

The equilibrium pressure and temperature of the three phases (hydrate (H)−water-rich liquid (L_W)−vapor (V)) in the silica gel pores should be determined by considering the pore-size distribution of the silica gels. For the gas hydrates of a single guest, the dissociation equilibrium point in silica gel pores was chosen as the inflection point of the pressure (P) versus temperature (T) heating curve, which corresponds to the equilibrium dissociation point in the pores of the mean diameter (d_{mean}) of the silica gels as suggested by Anderson et al.[7] and Seo et al.[8] However, for the mixed gas hydrates or hydrates made from electrolyte solutions, the inflection point of the P versus T heating curve does not correspond to the initial gas composition or electrolyte concentration. For systems with mixed gas hydrates or with an electrolyte present, the gas-phase composition of the mixed gas hydrates or electrolyte concentration in the liquid water phase becomes equal to the initial conditions only at the point of final pore hydrate dissociation, that is, maximum pore diameter (d_{max}). Figure 2 shows one example of the P versus T heating curve for the CH_4 (90%) + C_2H_6 (7%) + C_3H_8 (3%) + NaCl (3 wt %) + water mixtures in 56.6 (30.0) nm silica gel pores. To accurately account for pore size distribution, initial gas composition, and initial electrolyte concentration, the hydrate dissociation equilibrium point in silica pores was chosen in the present study as the final pore hydrate dissociation point that corresponds to the hydrate dissociation

at d_{max}. A more detailed explanation for determining the hydrate dissociation equilibrium point at d_{mean} or d_{max} was given in the previous papers.[8,12]

To identify the hydrate structure and to estimate the cage occupancy of guest molecules in the mixed CH_4 (90%) + C_2H_6 (7%) + C_3H_8 (3%) gas hydrate, a Bruker 400 MHz solid-state NMR spectrometer that belongs to the Korea Basic Science Institute (KBSI) was used in this study. The NMR spectra were recorded at 243 K by placing the hydrate samples within a 4 mm outer diameter (o.d.) Zr-rotor that was loaded into the variable temperature (VT) probe. All ^{13}C NMR spectra were recorded at a Larmor frequency of 100.6 MHz with magic angle spinning (MAS) at about 2−4 kHz. The pulse length of 2 μs and pulse repetition delay of 10 s under proton decoupling were employed when the radio frequency field strengths of 50 kHz corresponding to 5 μs 90° pulses were used. The downfield carbon resonance peak of adamantane, assigned a chemical shift of 38.3 ppm at 300 K, was used as an external chemical shift reference. The hydrate samples for NMR analysis were prepared with the same apparatus as that used for hydrate phase equilibrium measurement. When gas hydrate formation was completed, the formed gas hydrates were finely powdered in the liquid nitrogen vessel and sampled into Zr-rotor immersed in liquid nitrogen to prevent any gas hydrate dissociation. A more detailed description of experimental apparatus and procedure was given in previous papers.[6,8,12]

Results and Discussion

In narrow pores saturated with water, the depression of water activity induced by the partial ordering and bonding of water molecules with hydrophilic surfaces results in hydrate inhibition which requires that hydrate dissociation occurs at a higher pressure for any given temperature, or at a lower temperature for any given pressure, when compared with bulk conditions.[3] A similar situation applies to the ice−water transition where the freezing point of water in narrow pores is depressed relative to the bulk freezing point.[3] Three-phase H−L_W−V equilibria for the quaternary CH_4 (90%) + C_2H_6 (7%) + C_3H_8 (3%) + water mixtures in 12.9 (6.0), 22.6 (15.0), and 56.6 (30.0) nm silica gel pores were measured and presented in Figure 3 and Table 1. The capillary effect due to the presence of geometrical constraints caused the H−L_W−V equilibrium curves to be shifted to the inhibition region when compared with the bulk state. Results clearly indicate that the capillary inhibition effect of smaller pores on hydrate equilibrium dissociation conditions was more noticeable.

The operative interface of the hydrate and liquid water phases is crucial in understanding the pore effect on the hydrate formation/dissociation and calculating the activity of water in silica gel pores. However, no literature value of the mixed CH_4 + C_2H_6 + C_3H_8 gas hydrate−water interfacial tension (σ_{HW}) has been presented. To obtain the value of the gas hydrate−water interfacial tension, the Gibbs−Thomson equation, which relates the dissociation temperature depression (from bulk conditions) with the pore size of silica gels at a given pressure, was used in this study. According to this relationship, the temperature depression of hydrate dissociation in a cylindrical pore, $\Delta T_{m,pore}$, relative to the bulk dissociation temperature, $T_{m,bulk}$, is defined as[3,7]

$$\frac{\Delta T_{m,pore}}{T_{m,bulk}} = -\left(\frac{2\sigma_{HW}\cos\theta}{\rho_h \Delta H_{h,d} d}\right) \quad (1)$$

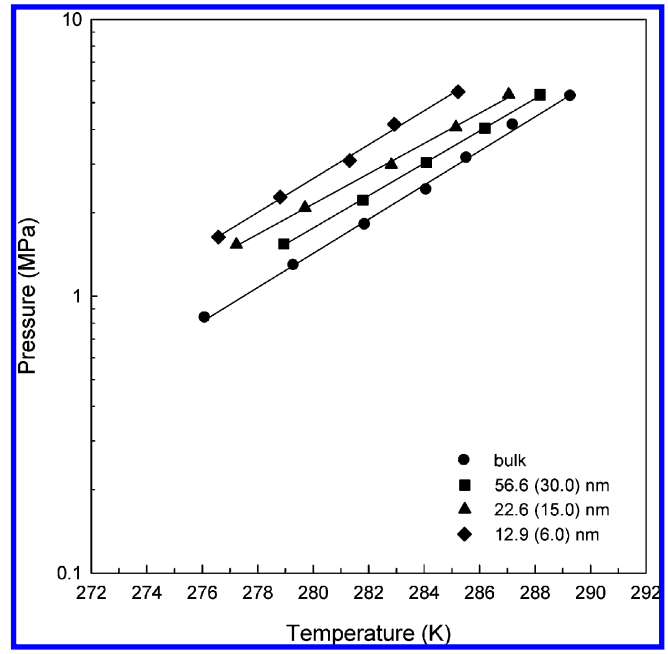

Figure 3. Hydrate phase equilibria of the quaternary CH_4 (90%) + C_2H_6 (7%) + C_3H_8 (3%) + water mixtures in silica gel pores.

where $\Delta T_{m,pore}$ is the difference between the pore ($T_{m,\ pore}$) and bulk dissociation temperature, $T_{m,bulk}$, at a specified pressure, ρ_h the hydrate density, $\Delta H_{h,d}$ the hydrate dissociation enthalpy, and d the pore diameter.

As can be seen in Figure 4, the interfacial tension between the hydrate and the water phase can be estimated from the slope of the plot of the reciprocal pore diameter ($1/d$) versus $\Delta T_{m,pore}/T_{m,bulk}$ for hydrate dissociation in silica gel pores on the basis of the experimental data shown in Figure 3. For the mixed CH_4 + C_2H_6 + C_3H_8 gas hydrate a value of $\Delta H_{h,d}$ = 79.2 kJ/mol was given using the Clausius−Clapeyron equation with the pressure−temperature data of three-phase H−L_W−V equilibrium, and a hydrate density can be assumed to be 940 kg/m^3 from the cage occupancies obtained by thermodynamic modeling in the literature.[1] Applying all of these values to eq 1, an average value for the mixed CH_4 (90%) + C_2H_6 (7%) + C_3H_8 (3%) gas hydrate−water interfacial tension of 47 ± 4 mJ/m^2 was obtained from the slope of data in Figure 4. This value is larger than that of CH_4 hydrate−water interfacial tension, 32 ± 1 mJ/m^2, and that of C_2H_6 hydrate−water interfacial tension, 39 ± 2 mJ/m^2, while this value is quite similar to that of C_3H_8 hydrate−water interfacial tension, 45 ± 1 mJ/m^2, and that of CH_4 (90%) + C_3H_8 (10%) hydrate−water interfacial tension, 42 ± 3 mJ/m^2, within the upper and lower error boundaries.[7,8,12] From the above results, it seems that the value of the hydrate−water interfacial tension mainly depends on the hydrate structure and cage occupancies of guest components because $\Delta H_{h,d}$, which is not only a function of crystal structure but also a function of cage occupancies, is the most dominant term in determining the slope of the plot of $\Delta T_{m,pore}/T_{m,bulk}$ versus $1/d$ in eq 1.

Three-phase H−L_W−V equilibria for the quinary CH_4 (90%) + C_2H_6 (7%) + C_3H_8 (3%) + NaCl + water mixtures in 56.6 (30.0) nm silica gel pores at NaCl concentrations of 3 and 10 wt % were measured and presented in Figure 5 and Table 2. As can be seen from Figure 5, pores and electrolytes themselves can inhibit gas hydrate formation. The combined effects of pores and electrolytes were also observed through examining the shift of the experimentally measured H−L_W−V equilibrium lines. As can be seen in Figures 3 and 5, the H−L_W−V equilibrium

TABLE 1: Hydrate Phase Equilibrium Data for the CH_4 (90%) + C_2H_6 (7%) + C_3H_8 (3%) + Water Mixtures in Silica Gel Pores

12.9 (6.0) nm		22.6 (15.9) nm		56.6 (30.0) nm		bulk	
T (K)	*P* (MPa)	*T* (K)	*P* (MPa)	*T* (K)	*P* (MPa)	*T* (K)	*P* (MPa)
276.58	1.635	277.23	1.534	278.94	1.544	276.09	0.837
278.81	2.282	279.70	2.088	281.79	2.22	279.29	1.294
281.31	3.088	282.82	2.983	284.09	3.043	281.86	1.817
282.93	4.176	285.15	4.073	286.19	4.041	284.08	2.426
285.23	5.474	287.05	5.353	288.18	5.333	285.53	3.162
						287.20	4.162
						289.28	5.284

lines were shifted more to the inhibition region when compared with the ones in the either bulk or pure state as the pore size decreased and electrolyte concentration increased. Gas hydrates need a higher pressure for stability both within the pores and in the presence of electrolytes. It is generally accepted that capillary inhibition due to the presence of geometrical constraints is considered to be equivalent to electrolyte inhibition.[2] Therefore, capillary inhibition is comparable to that resulting from the depression of the activity of water, which is induced by electrolytes. In the solid-solution model, equilibrium conditions of hydrates are directly influenced by the activity of water. As the activity of water decreases, the hydrates need a higher pressure for stability at a specified temperature or lower temperature for stability at a specified pressure.

With respect to the natural gas hydrate in the deep ocean sediment of fine-grained clay, the activity of water is first affected by electrolytes dissolved in the seawater and is further affected by the capillary force due to the sediment pores. For this reason, the combined effect of pores and electrolytes could be sufficient to shift a hydrate stability zone predicted without considering the inhibition of both pores and electrolytes. Therefore, it should be noted that laboratory experimental results dealing with only pure methane hydrate and bulk water cannot be directly applicable to natural gas hydrates, especially those deposited in sediments of fine-grained sand or clay.

In the present study, a ^{13}C MAS NMR experiment was carried out to analyze the solid hydrate phase of the mixed gas hydrate because NMR spectroscopy has been recognized as a powerful tool for the structure identification and quantitative determination of hydrate composition and cage occupancy.[13] In particular, the cage-dependent ^{13}C NMR chemical shifts for the enclathrated guest molecules can be used to determine structure types of the formed gas hydrates. Figure 6 shows a stacked plot of the ^{13}C MAS NMR spectra of pure CH_4, pure C_2H_6, pure C_3H_8, bulk CH_4 + C_2H_6 + C_3H_8, and pore CH_4 + C_2H_6 + C_3H_8 hydrates. Pure CH_4 hydrate (sI) spectrum has two resonance peaks at −4.3 and −6.6 ppm, respectively. The peak at −4.3 ppm can be assigned to CH_4 molecules in the small 5^{12} cages and the peak at −6.6 ppm to CH_4 molecules in the large $5^{12}6^2$ cage considering the ideal stoichiometric ratio of the small 5^{12} to the large $5^{12}6^2$ cages in the unit cell of sI. On the other hand, pure C_2H_6 hydrate, known to form sI, showed only one peak at 7.3 ppm, which can be assigned to C_2H_6 molecules captured in

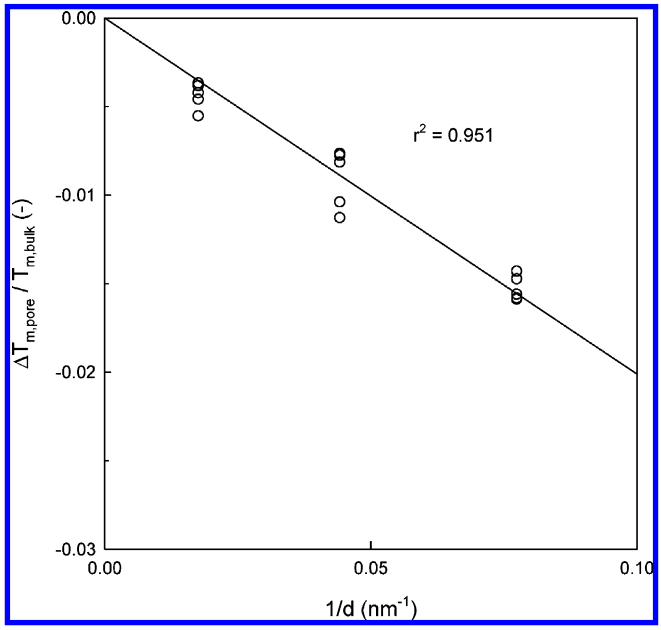

Figure 4. Plot of the reciprocal pore diameter (1/*d*) versus $\Delta T_{m,pore}/T_{m,bulk}$ for the mixed CH_4 (90%) + C_2H_6 (7%) + C_3H_8 (3%) hydrates in silica gel pores.

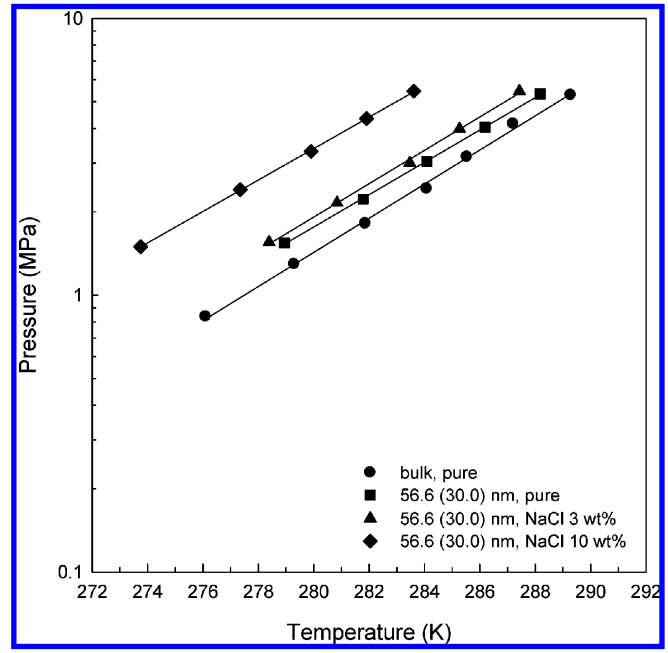

Figure 5. Hydrate phase equilibria of the quinary CH_4 (90%) + C_2H_6 (7%) + C_3H_8 (3%) + NaCl + water mixtures in silica gel pores.

TABLE 2: Hydrate Phase Equilibrium Data for the CH_4 (90%) + C_2H_6 (7%) + C_3H_8 (3%) + NaCl + Water Mixtures in 56.6 (30.0) nm Silica Gel Pores

pure		NaCl 3 wt %		NaCl 10 wt %	
T (K)	*P* (MPa)	*T* (K)	*P* (MPa)	*T* (K)	*P* (MPa)
278.94	1.544	278.39	1.552	273.75	1.498
281.79	2.22	280.84	2.154	277.35	2.404
284.09	3.043	283.47	2.999	279.90	3.305
286.19	4.041	285.26	3.984	281.91	4.344
288.18	5.333	287.43	5.457	283.62	5.457

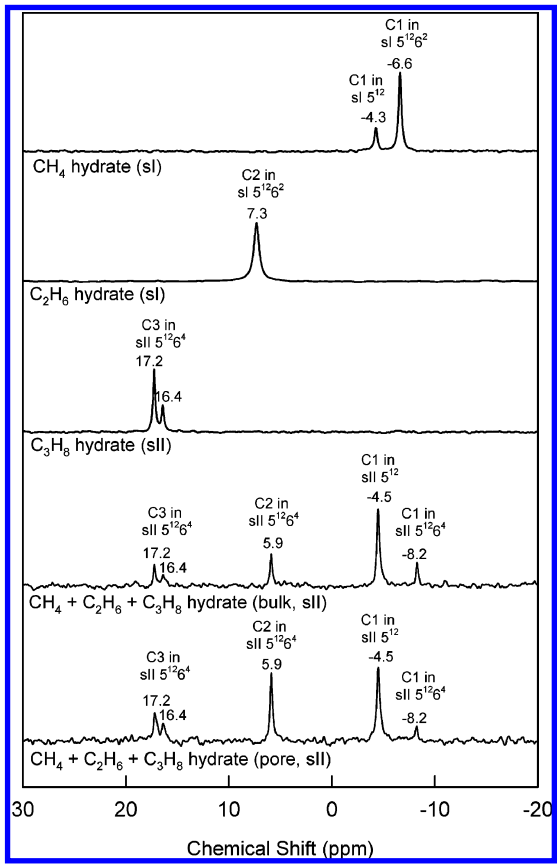

Figure 6. ^{13}C NMR spectra of the pure CH_4 (274.15 K and 10.0 MPa), pure C_2H_6 (274.15 K and 2.0 MPa), pure C_3H_8 (274.15 K and 0.3 MPa), bulk CH_4 (90%) + C_2H_6 (7%) + C_3H_8 (3%), and pore CH_4 (90%) + C_2H_6 (7%) + C_3H_8 (3%) gas hydrates. (The mixed gas hydrates in both bulk and pore states were formed at 284.15 K and 6.0 MPa.)

only large $5^{12}6^2$ cages of sI. For C_2H_6 hydrate, small 5^{12} cages are vacant because of the molecular size of C_2H_6. For the pure C_3H_8 hydrate, which is known to form sII, C_3H_8 molecules captured only in the large $5^{12}6^4$ cages of sII were identified by two distinct resonance lines, one from $-CH_2-$ (at 16.4 ppm) and the other from CH_3- (at 17.2 ppm). Therefore, the mixed $CH_4 + C_2H_6 + C_3H_8$ hydrate is confirmed to be sII from the fact that the positions of two distinct resonance peaks from captured C_3H_8 molecules are the same as those in the pure C_3H_8 hydrate. In the mixed $CH_4 + C_2H_6 + C_3H_8$ hydrate, the resonance peaks of CH_4 molecules in hydrate cages were exhibited at −4.5 and −8.2 ppm, indicating that CH_4 molecules occupy both the small and the large cages of sII. The resonance peak from CH_4 molecules in small 5^{12} cages of sII is located very near that in small 5^{12} cages of sI because both small cages of sI and sII consist of the pentagonal dodecahedra (5^{12}) of nearly the same dimension. However, because of the different size and shape of each large cage, a distinctive discrepancy between the chemical shifts of CH_4 molecules in the large $5^{12}6^2$ (at −6.6 ppm) of sI and $5^{12}6^4$ (at −8.2 ppm) of sII was observed, which can be effectively used as a clear indicator for determining the hydrate structure types. In the mixed $CH_4 + C_2H_6 + C_3H_8$ hydrate, the resonance peak at 5.9 ppm can be assigned to C_2H_6 molecules captured in large $5^{12}6^4$ cages of sII, which can also be used as a good indicator for sII hydrate formation. The NMR chemical shifts of the present study for enclathrated CH_4, C_2H_6, and C_3H_8 molecules are identical to those of literature reports.[12,14,15]

The cage occupancies of the mixed $CH_4 + C_2H_6 + C_3H_8$ hydrate components are calculated from the relative integrated intensities of ^{13}C MAS NMR signals at each chemical shift combined with the following statistical thermodynamic expression representing the chemical potential of water molecules. In the absence of guest−guest interactions and host-lattice distortions, the chemical potentials of water molecules of sI and sII are, respectively, given by[16]

$$\mu_W(h) - \mu_W(h^0) = \frac{RT}{23}[3\ln(1 - \theta_{l,CH_4}) + \ln(1 - \theta_{s,CH_4})] \quad (2)$$

$$\mu_W(h) - \mu_W(h^0) = \frac{RT}{17}[\ln(1 - \theta_{l,C_3H_8} - \theta_{l,C_2H_6} - \theta_{l,CH_4}) + 2\ln(1 - \theta_{s,CH_4})] \quad (3)$$

where $\mu_W(h^0)$ is the chemical potential of water molecules of a hypothetical empty lattice and θ_s and θ_l are the fractional occupancies of small and large cages, respectively. When the gas hydrate is in equilibrium with ice, the left side of the above equation becomes $\mu_W(\text{ice}) - \mu_W(h^0) = -\Delta\mu_W^0$ where $\Delta\mu_W^0$ is the chemical potential of the empty lattice relative to ice. The values of $\Delta\mu_W^0$ used in this work are 1297 J/mol for sI and 883.8 J/mol for sII.[1] The integrated intensity ratios of guest CH_4 to C_2H_6 and C_3H_8 molecules were substituted in the above equations to calculate the cage occupancies of each molecule, and the results were listed in Table 3. For both bulk and pore $CH_4 + C_2H_6 + C_3H_8$ hydrates, small cages were only occupied by CH_4 molecules, while large cages are shared by CH_4, C_2H_6, and C_3H_8 molecules. However, as indicated by Seo et al.,[15] we also note that for large cages the cage occupancies of C_2H_6 and C_3H_8 molecules in 56.6 (30.0) nm pores were higher than those in bulk state, which results from the preferential transportation of heavier hydrocarbons such as C_2H_6 and C_3H_8 inside silica gel pores and subsequent participation in the formation of mixed gas hydrate by occupying a large number of sII large cages.

Using the cage occupancies obtained above, we can calculate the hydration number by the following expression:

$$n = \frac{136}{16\theta_{s,CH_4} + 8(\theta_{l,CH_4} + \theta_{l,C_2H_6} + \theta_{l,C_3H_8})} \quad (4)$$

The hydration numbers of each system obtained from eq 4 were listed along with the cage occupancies in Table 3. The values of cage occupancies and hydration numbers obtained by ^{13}C MAS NMR are generally in good agreement with literature values even though there is slight deviation because of difference in initial gas compositions and experimental conditions.[15,17,18]

TABLE 3: Cage Occupancies of the Pure CH_4 and Mixed CH_4 (90%) + C_2H_6 (7%) + C_3H_8 (3%) Hydrates

		CH_4		C_2H_6	C_3H_8	hydration number
system	structure	θ_{s,CH_4}	θ_{l,CH_4}	θ_{l,C_2H_6}	θ_{l,C_3H_8}	n
CH_4 + water	sI	0.894	0.974	–	–	6.03
$CH_4 + C_2H_6 + C_3H_8$ + water (bulk)	sII	0.873	0.428	0.270	0.220	6.38
$CH_4 + C_2H_6 + C_3H_8$ + water (56.6 (30.0) nm)	sII	0.703	0.232	0.486	0.267	7.11

Conclusions

The phase behavior and structural details of the pore CH_4 (90%) + C_2H_6 (7%) + C_3H_8 (3%) hydrates were closely investigated through experimental measurements of the three-phase H−L_W−V equilibria and ^{13}C NMR spectra. The H−L_W−V equilibrium lines were shifted more toward the inhibition region when compared with the ones in the either bulk or pure state as the pore size decreased and NaCl concentration increased. Through the Gibbs−Thomson equation for dissociation within the cylindrical pores, the value of the CH_4 + C_2H_6 + C_3H_8 hydrate−water interfacial tension (σ_{HW}) was found to be 47 ± 4 mJ/m^2. It can be concluded that the structure of the mixed CH_4 (90%) + C_2H_6 (7%) + C_3H_8 (3%) hydrate is sII and that small cages are occupied only by CH_4 molecules, whereas large cages were shared by CH_4, C_2H_6, and C_3H_8 molecules. The overall thermodynamic and spectroscopic results obtained in this study can be used for understanding the fundamental phase behavior and structural characteristics of the mixed pore gas hydrates in the presence of electrolytes and, thus, could be applied as valuable information in exploring and exploiting the natural gas hydrates in marine sediments.

Acknowledgment. This work was supported by the Human Resources Development Program of the Korea Institute of Energy Technology Evaluation and Planning (KETEP) Grant funded by the Korea government Ministry of Knowledge Economy and was also supported by the Basic Science Research Program through the National Research Foundation of Korea (NRF) funded by the Ministry of Education, Science and Technology (2009-0069569).

References and Notes

(1) Sloan, E. D.; Koh, C. A. *Clathrate Hydrates of Natural Gases*, 3rd ed.; CRC Press: Boca Raton, FL, 2008.

(2) Handa, Y. P.; Stupin, D. *J. Phys. Chem.* **1992**, *96*, 8599–8603.

(3) Clennell, M. B.; Hovland, M.; Booth, J. S.; Henry, P.; Winters, W. J. *J. Geophys. Res.* **1999**, *104*, 22985–23003.

(4) Smith, D. H.; Wilder, J. W.; Seshadri, K. *AIChE J.* **2002**, *48*, 393–400.

(5) Uchida, T.; Ebinuma, T.; Takeya, S.; Nagao, J.; Narita, H. *J. Phys. Chem. B* **2002**, *106*, 820–826.

(6) Seo, Y.; Lee, H.; Uchida, T. *Langmuir* **2002**, *18*, 9164–9170.

(7) Anderson, R.; Llamedo, M.; Tohidi, B.; Burgass, R. W. *J. Phys. Chem. B* **2003**, *107*, 3507–3514.

(8) Seo, Y.; Lee, S.; Cha, I.; Lee, J. D.; Lee, H. *J. Phys. Chem. B* **2009**, *113*, 5487–5492.

(9) Dholabhai, P. D.; Englezos, P.; Kalogerakis, N.; Bishnoi, P. R. *Can. J. Chem. Eng.* **1991**, *69*, 800–805.

(10) Østergaard, K. K.; Anderson, R.; Llamedo, M.; Tohidi, B. *Terra Nova* **2002**, *14*, 307–312.

(11) Seo, Y.; Lee, H. *J. Phys. Chem. B* **2003**, *107*, 889–894.

(12) Lee, S.; Seo, Y. *Langmuir* **2010**, *26*, 9742–9748.

(13) Ripmeester, J. A.; Ratcliffe, C. I. *J. Struct. Chem.* **1999**, *40*, 654–662.

(14) Kim, D. Y.; Lee, J.-W.; Seo, Y. T.; Ripmeester, J. A.; Lee, H. *Angew. Chem., Int. Ed.* **2005**, *44*, 7749–7752.

(15) Seo, Y.; Kang, S. P.; Jang, W. *J. Phys. Chem. A* **2009**, *113*, 9641–9649.

(16) van der Waals, J. H.; Platteeuw, J. C. *Adv. Chem. Phys.* **1959**, *2*, 1–58.

(17) Uchida, T.; Takeya, S.; Kamata, Y.; Ohmura, R.; Narita, H. *Ind. Eng. Chem. Res.* **2007**, *46*, 5080–5087.

(18) Kumar, R.; Linga, P.; Moudrakovski, I.; Ripmeester, J. A.; Englezos, P. *AIChE J.* **2008**, *54*, 2132–2144.

JP108037M